

# In Situ Study of Microstructure Evolution in Solidification of Hypereutectic Al-Si Alloys with Application of Thermal Analysis and Neutron Diffraction



DIMITRY G. SEDIAKO and WOJCIECH KASPRZAK

Understanding of the kinetics of solid-phase evolution in solidification of hypereutectic aluminum alloys is a key to control their as-cast microstructure and resultant mechanical properties, and in turn, to enhance the service characteristics of actual components. This study was performed to evaluate the solidification kinetics for three P-modified hypereutectic Al-19 pct Si alloys: namely, Al-Si binary alloy and with the subsequent addition of 2.8 pct Cu and 2.8 pct Cu + 0.7 pct Mg. Metallurgical evaluation included thermodynamic calculations of the solidification process using the FactSage™ 6.2 software package, as well as experimental thermal analysis, and *in situ* neutron diffraction. The study revealed kinetics of solid  $\alpha$ -Al, solid Si,  $\text{Al}_2\text{Cu}$ , and  $\text{Mg}_2\text{Si}$  evolution, as well as the individual effects of Cu and Mg alloying additions on the solidification path of the Al-Si system. Various techniques applied in this study resulted in some discrepancies in the results. For example, the FactSage computations, in general, resulted in 281 K to 286 K (8 °C to 13 °C) higher Al-Si eutectic temperatures than the ones recorded in the thermal analysis, which are also ~278 K (~5 °C) higher than those observed in the *in situ* neutron diffraction. None of the techniques can provide a definite value for the solidus temperature, as this is affected by the chosen calculation path [283 K to 303 K (10 °C to 30 °C) higher for equilibrium solidification vs non-equilibrium] for the FactSage analysis; and further complicated by evolution of secondary Al-Cu and Mg-Si phases that commenced at the end of solidification. An explanation of the discrepancies observed and complications associated with every technique applied is offered in the paper.

DOI: 10.1007/s11661-015-3007-0

© Published with permission of Her Majesty the Queen in Right of Canada, as represented by the Minister of Natural Resources 2015

## I. INTRODUCTION

HYPEREUTECTIC Al-Si alloys containing up to 16 to 20 pct Si exhibit attractive service properties under conditions of high temperature, tension and compression load cycles, and vibration. These alloys are extensively used for demanding applications in the automotive industry where superior tribological performance under high operating temperatures is required.<sup>[1-6]</sup>

In addition to being light weight, such alloys have good thermal conductivity and are utilized for rapid heat removal in internal combustion engines. Examples of components include monolithic engine blocks cast using high-pressure die casting (HPDC), cylinder bore inserts for sand cast engine blocks, engine pistons made using low-pressure permanent mold (LPPM), and hot forgings.

Typically, hypereutectic alloys contain, in addition to about 16 to 20 pct Si, up to 3 pct Cu and up to 0.5 pct Mg, which are added to increase strength *via* the precipitation strengthening mechanism. In addition, 0.01 pct P is used in order to achieve uniform size, shape, and distribution of the primary Si crystals that nucleate on  $\text{AlP}_3$  particles during the alloy solidification process. Under equilibrium or semi-equilibrium conditions, the microstructure of this alloy consists of  $\alpha$ -Al dendrites, primary Si, Al-Si eutectic, Fe-based phases as well as Cu- or Mg-based intermetallics, *i.e.*,  $\text{Al}_3\text{FeSi}$ ,  $\text{Al}_8\text{Mg}_3\text{FeSi}_6$ ,  $\text{Al}_5\text{Mg}_8\text{Cu}_2\text{Si}_6$ .<sup>[7-9]</sup> Secondary phases precipitate during heat treatment processing, that is,  $\text{AlCu}_2$  and  $\text{Mg}_2\text{Si}$  which are present with morphologies and in quantities depending on given heat treatment parameters.

Commercial hypereutectic alloys contain typically up to 20 pct of Si but some research studies focused on higher concentrations. Early studies in the 1960s were conducted by Gosh and Telang for binary-type Al-Si alloy system containing up to 22 pct Si and up to 0.2 pct phosphorus. These studies focused predominantly on fundamentals of the primary Si refinement as well as the effect of melt processing parameters. It was found that melt heating above approximately 1173 K (900 °C) prior to casting resulted in coarsening of the primary

DIMITRY G. SEDIAKO, Senior Research Officer, is with the Canadian Neutron Beam Centre, Chalk River, ON, Canada. Contact e-mail: dimitry.sediako@cnl.ca WOJCIECH KASPRZAK, Director of Operations, is with the CanmetMATERIALS, Natural Resources Canada, 183 Longwood Road South, Hamilton, ON, Canada.

Manuscript submitted August 9, 2013.

Article published online July 2, 2015

Si for the test sample solidified inside the water cooled steel crucible. It was suggested that the AIP particles started to disintegrate or even melt above 1173 K (900 °C) and caused a coarsening effect of primary Si crystals.<sup>[10,11]</sup> Intensive research in the 1980s led to commercial application of hypereutectic alloy in engine blocks in passenger vehicles.<sup>[12,13]</sup> These engine blocks were cast using the low-pressure die casting process. On the other hand, advancements in high-pressure die casting technologies resulted in the commercial application of DiASiI™ in the production of liner-less engine blocks for motorcycle application. Control of primary Si size and distribution was one of the key challenges to be addressed. Due to reduction of porosity using vacuum processing, these engine blocks are heat treated now using traditional T6 temper.<sup>[14]</sup> Further optimization of heat treatment processing enabled development of energy efficient tempering routes.<sup>[15]</sup>

Since adequate refinement of the primary Si crystals is of key importance and creates a technological challenge particularly during casting manufacturing, microstructure control methods represent a key research theme.<sup>[16]</sup> Currently, the scientific focus is on refinement of the primary Si crystals achieved by controlled alloying, addition of master alloys, and rapid solidification. Research interests are also centered on mechanical, electromagnetic and ultrasonic melt treatment techniques used to modify the primary Si crystals as well as other structural constituents.<sup>[3,17–19]</sup> Powder metallurgy offered an alternative method to achieve satisfactory refinement of the primary Si crystals. However, due to its prohibitive cost, powder metallurgy is used only for selected applications.

Despite extensive studies conducted so far, the exact metallurgical mechanisms that control the solidification kinetics are still not well understood, partially due to a lack of investigation techniques suitable for *in situ* analysis of microstructure development during the solidification process that is representative of a given casting process. For this reason, novel testing techniques for alloy and manufacturing process evaluation are needed to develop components capable to meet future performance requirements.

Significant residual stress may frequently develop during the solidification of complex automotive components. Residual stress is affected by geometry of the castings, cooling rates and microstructure, and the phases that have evolved during solidification.<sup>[20]</sup> Many studies have been performed on the solidification behavior of these alloys and the resulting as-cast microstructure. Most recently, neutron diffraction<sup>[21–25]</sup> in conjunction with thermal analysis<sup>[3–5]</sup> were used to evaluate the solidification kinetics of hypereutectic Al-Si alloy under non-equilibrium and near-equilibrium conditions. In reports,<sup>[21,22]</sup> Iqbal *et al.* carried out time-dependent neutron diffraction measurements on the microstructure evolution of pure Al and Al-0.3 pct Ti-0.02 pct B alloy for different cooling rates. In these studies, the evolution of the static structure factor  $S(Q)$  was monitored during liquid-to-solid phase transformation as a function of the cooling rate. In the latter reports,<sup>[23–25]</sup> Kasprzak, Sediako *et al.* demonstrated the feasibility of using neutron diffraction to analyze solid-

ification of a binary hypereutectic Al-19 pct Si alloy using step-wise cooling. The authors demonstrated the potential to quantify the volume fraction of primary Si and Al, as well as Si and Al in the eutectic phase using diffraction signals from solid phases as they evolved during solidification.<sup>[23,24]</sup> These studies were extended into comparative analysis of solidification of the binary Al-19 pct Si alloy, and the same alloy modified with addition of 3 pct Cu.<sup>[25]</sup> As a result, these studies revealed major changes to the solidification path introduced by the addition of Cu.<sup>[26]</sup>

The current study continues this solidification analysis, extending it to a hypereutectic Al-19 pct Si alloy modified with the subsequent addition of 2.8 pct Cu and 0.7 pct Mg—an alloy that has similar composition to commercial alloys, *i.e.*, DiASiI™, or 390 used in manufacturing of automotive powertrain components.<sup>[22]</sup> This comparative analysis reveals changes to the solidification path caused by the addition of Mg to the Al-Si-Cu system. It is expected that this “dissecting” approach—from Al-Si to Al-Si-2.8 pct Cu to Al-Si-2.8 pct Cu-0.7 pct Mg—will lead to a better understanding of the effect of each alloying element on microstructure formation during solidification of complex alloying systems, thus enabling alloy chemistry to be tailored, to achieve the desired as-cast microstructure and corresponding mechanical properties.

## II. EXPERIMENTAL METHODOLOGY

### A. Chemical Composition of the Alloys

Four hypereutectic Al-Si alloys were analyzed in the present study; their composition is presented in Table I. The binary alloy (sample A) was selected to minimize the effect of other alloying elements on neutron diffraction and thermal analysis signals. Such an approach better validates the suitability of neutron diffraction techniques for solidification analysis.<sup>[24]</sup>

On the other hand, commercial hypereutectic alloys, such as 390, in addition to containing 16 to 19 pct Si, also contains additions of Cu up to 4 pct, Mg up to 1 pct, and P up to 0.1 pct. Such alloys are used for a number of most demanding applications in the automotive industry; *e.g.*, engine blocks and pistons manufactured using HPDC and LPPM technologies.<sup>[1–6]</sup> To characterize the individual effect of these alloying additions, the sample selection presented in Table I includes hypereutectic Al-Si alloys modified with and without 0.01 pct P (sample A and B), 2.8 pct Cu (sample C), and 0.7 pct Mg (sample D).

### B. Thermal Analysis and Neutron Diffraction During the Alloy Solidification Process

Thermal analysis performed in this study for the melting and solidification cycle for the selected alloys was carried out using the Universal Metallurgical Simulator and Analyzer (UMSA) Technology Platform.<sup>[27]</sup> The cylindrical-shaped test samples with an outer diameter of 16 mm and a length of 18 mm were

**Table I. Optical Emission Spectroscopy (OES) Results for the Selection of Hypereutectic Al-Si Alloys with the Addition of P, Cu, and Mg**

Sample ID	Chemical Composition (Weight Percent)					
	Si	Cu	Mg	Fe	Mn	P
A: Al-Si	19.5	0.01	<0.01	0.11	<0.01	—
B: Al-Si-P	18.6	0.01	<0.01	0.11	<0.01	0.01
C: Al-Si-Cu-P	18.7	2.8	<0.01	0.11	<0.01	0.01
D: Al-Si-Cu-Mg-P	17.7	2.8	0.7	0.11	<0.01	0.01

heated to  $785\text{ }^{\circ}\text{C} \pm 0.2\text{ }^{\circ}\text{C}$  and isothermally kept at this temperature for a period of 10 minutes to stabilize the melt temperature and homogeneity. Next, the test samples were solidified at an average cooling rate of about  $0.5\text{ }^{\circ}\text{C}/\text{s}$ , calculated between the non-equilibrium liquidus temperature (the start of the solidification process) and the non-equilibrium solidus temperature (the end of the solidification process). To analyze the phase transformation temperatures, the first derivative of the temperature with respect to time and the fraction solid (FS) were calculated and plotted against temperature. The detailed methodology is described in earlier publications.<sup>[3-5]</sup> The data obtained in the thermal analysis experiments were further verified by phase evolution calculations based on Gibbs energy minimization using the FactSage software package.<sup>[23-25]</sup> For the melting and solidification cycle, the program calculates the concentrations of chemical phases at the state of chemical equilibrium.<sup>[28]</sup>

The neutron diffraction studies on phase evolution during solidification were carried out using the C2 neutron powder diffractometer at the Canadian Neutron Beam Centre as well as the High-Resolution Powder Diffractometer installed at High Flux Isotope Reactor (HFIR) in Oak Ridge National Laboratories. In our earlier publication, we presented a detailed description of the methodology of these *in situ* experiments, as well as of the solidification cell that was designed and built to carry out controlled melting and solidification experiments during neutron diffraction.<sup>[25]</sup> Diffraction patterns were collected isothermally in the step-wise mode, holding for 30 minutes at the selected temperatures within the solidification interval. The measurements recorded scattered intensity *vs* scattering angle,  $2\Theta$ , where  $\Theta$  is the Bragg angle. The neutron wavelength used for these experiments was 0.154 nm and the analyzed scattering angle ranged from 20 to 120 deg.

### C. Microstructure and Mechanical Properties Evaluation

The microstructure examinations were carried out using an optical microscope and scanning electron microscope (SEM) in the SE and BSE mode. In addition to EDX chemical analyses, the electron probe microanalysis (EPMA) was used to analyze the concentration of alloying elements in various intermetallic phases. The alloy hardness was measured at room temperature using a Buehler Rockwell tester employing F scale and 60 kg load. For each sample, twenty measurements were conducted and an

average value along with the standard deviation was plotted. The room temperature uniaxial tensile tests were performed on the as-cast and heat treated samples following ASTM: E8/E8M-11 and ASTM: E9-09 standards at a strain rate of  $10^{-3}\text{ s}^{-1}$  using the computerized tensile testing machine. For graphical data representation, the average and standard deviation values of tensile, yield strength and elongation values were used.

## III. EVOLUTION OF SOLID PHASES DURING SOLIDIFICATION

### A. As-Cast Microstructure Characterization and Mechanical Properties

Microstructure observations of the binary Al-19 pct Si alloy under optical microscope (Figure 1(a)) revealed coarse and unmodified primary Si crystals (up to  $500\text{ }\mu\text{m}$ ) heterogeneously distributed in the as-cast microstructure (#1) as well as unmodified Al-Si eutectic (#2) and primary  $\alpha$ -Al dendrites (#3). As far as the alloy's technological properties are concerned, the presence of Al dendrites, which nucleate as a result of non-equilibrium solidification process, has negative impact on alloy machinability characteristics due to its significantly lower hardness as compared with other structural constituents.<sup>[1,5]</sup>

Addition of 0.01 pct P had a visible effect on the primary Si refinement level, depending on Cu and Mg additions for the given solidification conditions (Figures 1(b) through (d)). Subsequent addition of  $\sim 2.8$  pct Cu resulted in the formation of  $\text{AlCu}_2$  intermetallic phases, typically having blocky and eutectic morphology,<sup>[29]</sup> and subsequent addition of 0.7 pct Mg led to formation of the  $\text{Mg}_2\text{Si}$ , as well as  $\text{Q-Al}_5\text{Mg}_8\text{Si}_6\text{Cu}_2$  intermetallic phases. Such phases are typically observed in the Al-Si foundry alloys containing Cu and Mg additions<sup>[29,30]</sup> and were clearly visible on the SEM/SE images under low (Figures 2(a) and (c)) as well as higher magnification (Figures 2(b) and (d)).

Microstructural analysis clearly indicated that addition of Cu and Mg to Al-19 pct Si alloy having 0.01 pct P content resulted in progressive refinement of primary Si crystals. That is, the typical size of the primary Si crystals in the images decreased to approximately  $55\text{ }\mu\text{m}$  for Al-Si + P and to approximately  $40\text{ }\mu\text{m}$  for Al-Si + P + Cu + Mg additions. The individual role of Cu and Mg on primary Si refinement is not well reported in the literature and requires further studies. The EPMA

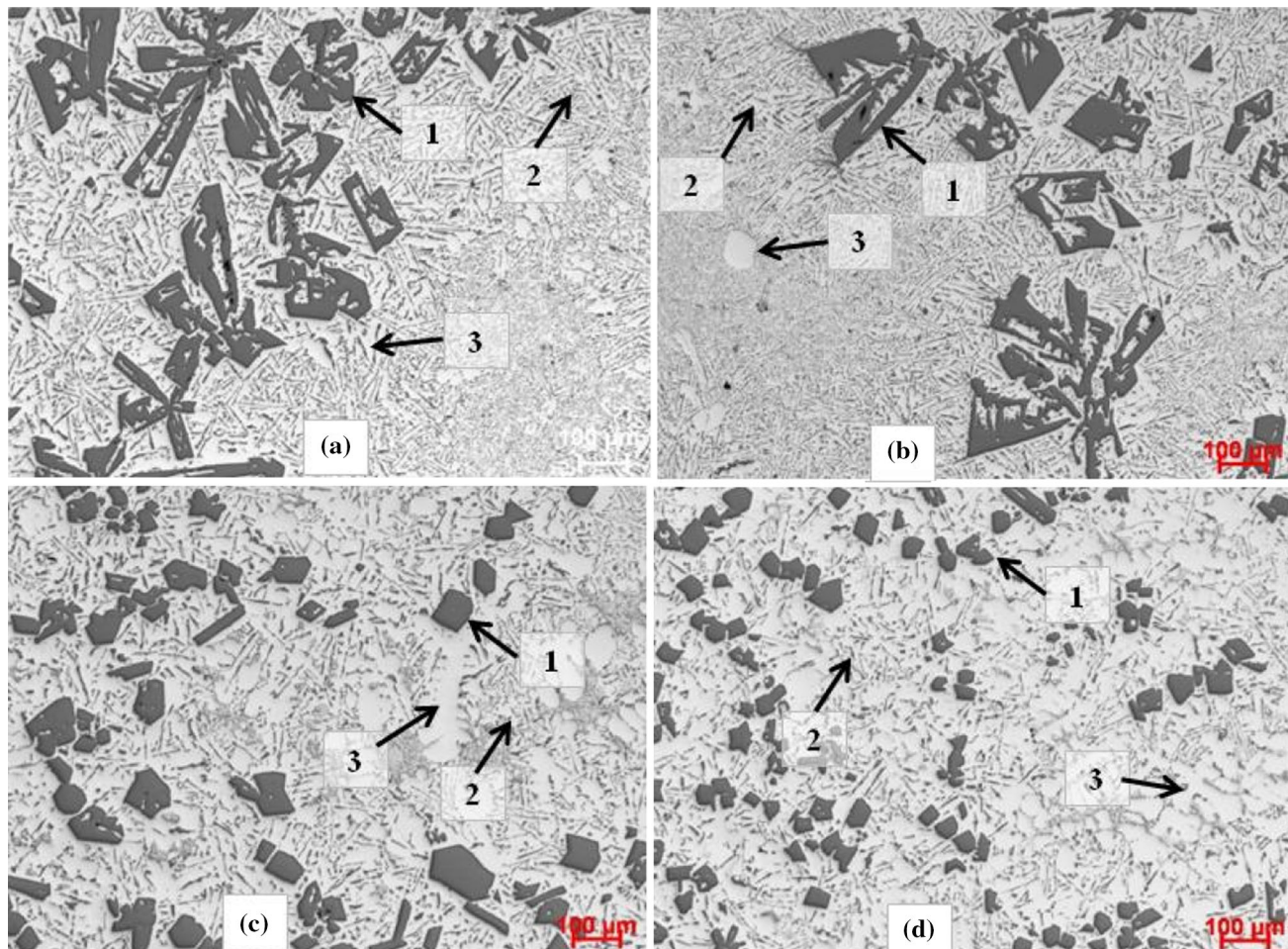


Fig. 1—As-cast microstructure under light optical microscope: (a) Al-19 pct Si, (b) Al-19 pct Si-0.01 pct P, (c) Al-19 pct Si-0.01 pct P-2.8 pct Cu, (d) Al-19 pct Si-0.01 pct P-2.8 pct Cu-0.7 pct Mg. Examples of structural constituents are numbered as follows: primary Si crystals (#1), the Al-Si (#2) and  $\alpha$ -Al dendrites (#3). The level of primary Si modification remains similar with addition of 0.01 pct of P (b) and undergoes progressive refinement with subsequent addition of 2.8 pct Cu (c) and 0.7 pct Mg (d).<sup>[3]</sup>

analysis of the primary Si crystals confirmed the presence of Cu in concentration up to 0.33 pct and Al up to 0.18 pct indicating a possible effect of these alloying elements on primary Si refinement level.<sup>[26]</sup>

It was also found that as-cast alloy hardness was not affected by addition of 0.01 pct P in the Al-19 pct Si alloy ( $24.5 \pm 2.7$  vs  $22.8 \pm 1.5$  HRB) but increased with the addition of Cu by approximately 25 HRB and with 0.7 pct Mg by a subsequent 15 HRB. A similar trend was observed for tensile strength, which increased from  $91 \pm 2$  MPa for Al-19 pct Si alloy to  $177 \pm 2$  MPa for alloy containing Cu and Mg additions, and which was accompanied by gradual decrease in elongation (Figure 3).<sup>[26]</sup>

Examples of structural constituents are numbered as follows: Al metal matrix (#1), primary Si crystals (#2), Al-Si eutectic (#3), Cu based phases ( $\text{Al}_2\text{Cu}$ , #4), Mg based phases ( $\text{Mg}_2\text{Si}$ , #5).<sup>[26]</sup>

Note the progressive increase in volume fraction of intermetallic phases observed under low magnification (a and c) with subsequent addition of 2.8 pct Cu (a and b) and 0.7 pct Mg (c and d).

## B. FactSage™ Calculations

In the research presented in Reference 25, the authors reviewed results of FactSage calculations compared to the experimental data obtained from *in situ* neutron diffraction and thermal analysis experiments conducted on a hypereutectic Al-19 pct Si-2.8 pct Cu alloy. It was demonstrated that, along with other metallurgical changes, Cu addition results in the formation of up to 2 pct of the  $\text{Al}_2\text{Cu}$  theta phase, either soon after complete solidification for equilibrium solidification [about 303 K (30 °C) below solidus], or immediately following complete solidification for the non-equilibrium process. This result was confirmed by observing a notable additional energy release within the temperature range of 763 K to 781 K (490 °C to 508 °C) in the thermal analysis (Figure 7, points #3 and 4). The authors also showed that formation of the theta phase is coupled with a reduction in Cu concentration in the FCC phase, from its maximum of 3.5 pct at 791 K (518 °C), to 2.5 pct at 728 K (455 °C).<sup>[25]</sup>

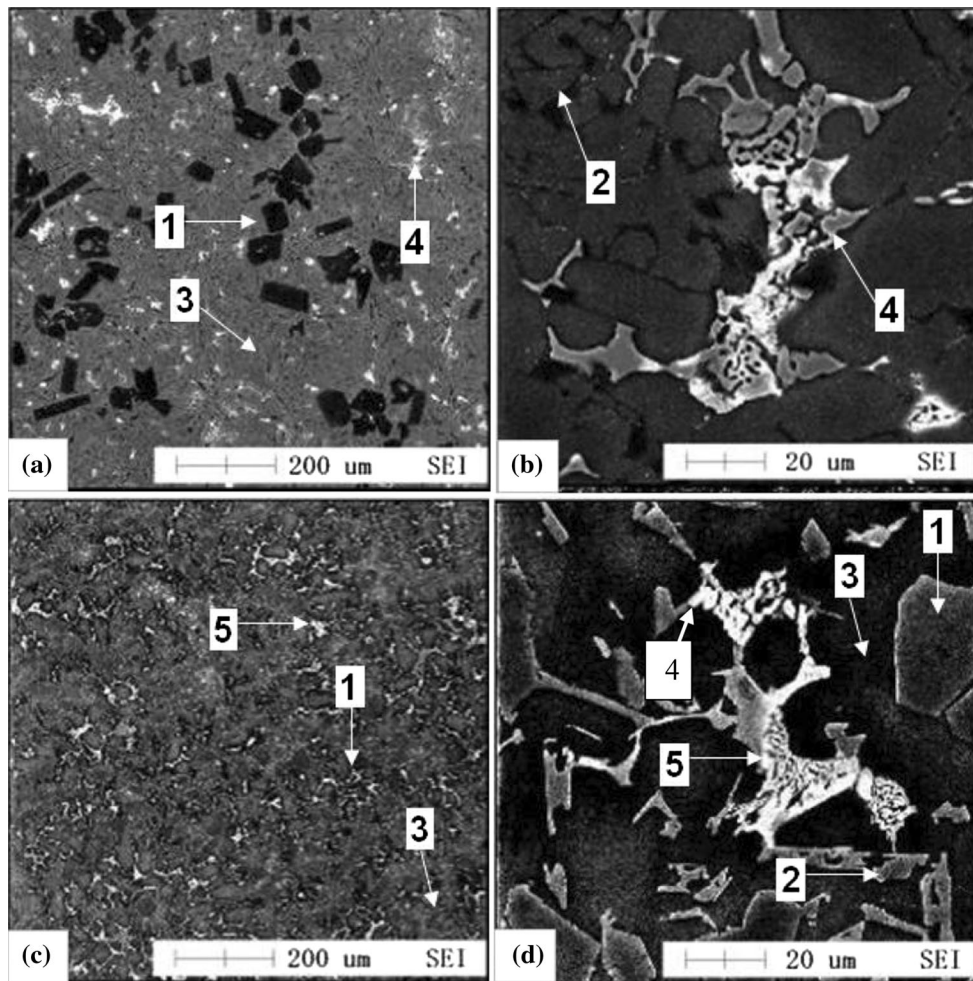


Fig. 2—As-cast microstructure observed under SEM in the SE mode: (a, b) Al-19 pct Si-0.01 pct P-2.8 pct Cu, (c, d) Al-19 pct Si-0.01 pct P-2.8 pct Cu-0.7 pct Mg.

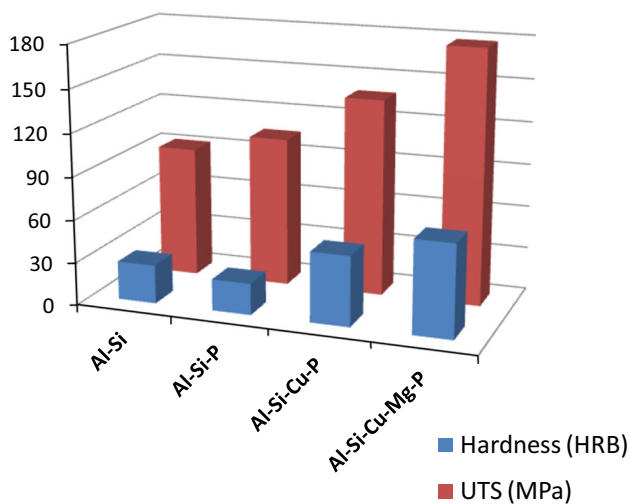


Fig. 3—As-cast hardness and ultimate tensile strength as a function of alloy chemistry.

Addition of 0.7 pct Mg further affects the solidification path. As depicted from the phase diagram presented in Figure 4 and the equilibrium solidification

presented in Figure 5, the solid FCC  $Mg_2Si$  phase starts evolving in the system about 283 K (10 °C) below the eutectic temperature of 841 K (568 °C). When the temperature is further reduced to 748 K (475 °C),  $Al_2Cu$  theta phase starts evolving concurrently with the  $Mg_2Si$  phase. The equilibrium calculations indicate that the initiation of theta phase formation occurs just prior to complete solidification of the alloy at the solidus temperature of 740 K (467 °C) (Figure 5(b)). Similar to the Al-19 pct Si-2.8 pct Cu alloy, formation of the theta phase in the Al-19 pct Si-2.8 pct Cu-0.7 pct Mg alloy occurs at the expense of reducing the Cu concentration in the FCC phase from, in this case, a maximum of 2.9 pct to about 2.3 pct at 723 K (450 °C).

FactSage computation results for the non-equilibrium solidification process based on the Scheil approach are shown in Figure 6. There is an obvious disadvantage to this approach. That is, the computations terminate when the amount of liquid phase in the system becomes 0 pct and, therefore, the kinetics of solid-state transformations that take place below the solidus temperature are missed entirely, as shown in Figure 6. The figure shows that for the two alloys under analysis, theta phase evolution occurs “all-at-once” at the solidus

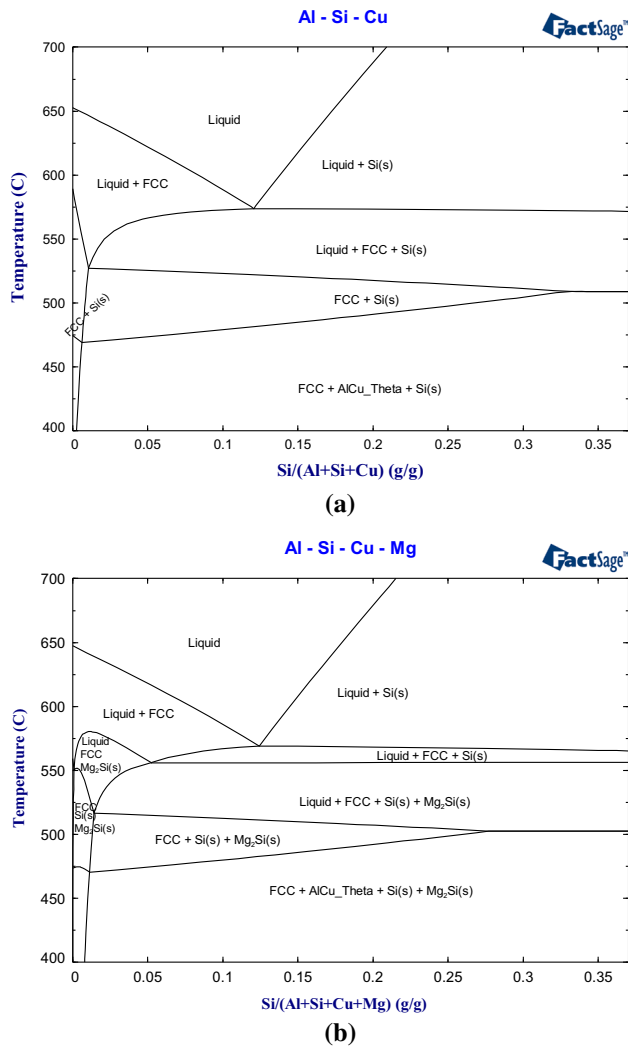


Fig. 4—Phase diagram for Al-19 pct Si-2.8 pct Cu (a) and Al-19 pct Si-2.8 pct Cu-0.7 pct pct Mg (b) alloys.

temperature; in both cases, the total amount of  $Al_2Cu$  is about 4 pct. On the contrary, the  $Mg_2Si$  phase starts forming at the end of solidification, about 283 K (10 °C) below the Al-Si eutectic, and its concentration just prior to the solidus temperature is 1.2 pct. At the solidus temperature, however, the total weight concentration of  $Mg_2Si$  is increased by an additional 0.2 to 1.4 pct. This increase coincides with a gradual increase in the amount of Mg and Si dissolved in the Al FCC phase to the total of 0.2 and 0.6 pct respectively, as shown in the zoomed-in 0-to-10 pct section (see Figure 6(c)) of the calculated path (Figure 6(b)).

The FactSage calculations simulate the complex solidification process, and are based on a number of approximations. As such, the calculations do not necessarily closely reflect the dynamics of the actual solidification process of the industrial type alloys. In order to gain a better understanding of the alloys' actual solidification processes, and also to verify the calculations, thermal analysis and *in situ* neutron diffraction

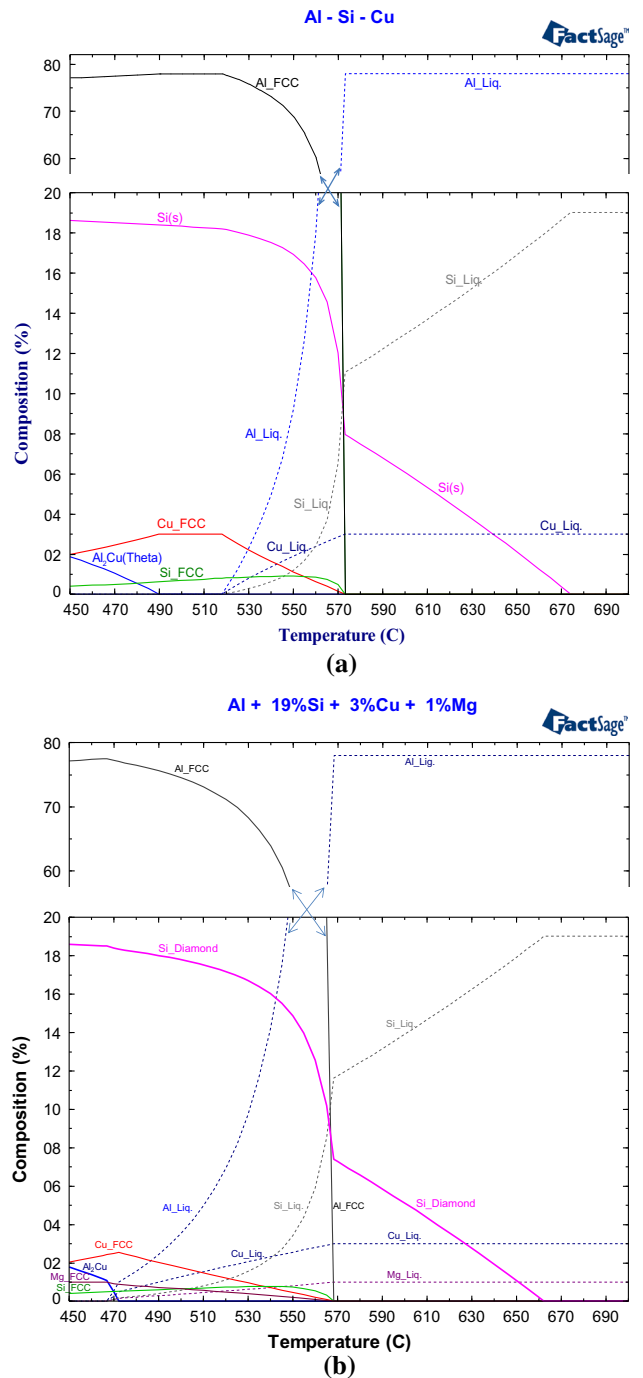


Fig. 5—FactSage calculation of equilibrium solidification for Al-19 pct Si-2.8 pct Cu alloy (a) and Al-19 pct Si-2.8 pct Cu-0.7 pct pct Mg alloy (b).

experiments on the solidification of the two selected alloys were performed.

### C. Thermal Analysis

The results of the thermal analysis of the cooling curves carried out for the Al-19 pct Si hypereutectic alloys are shown in Figure 7, which presents the temperature over

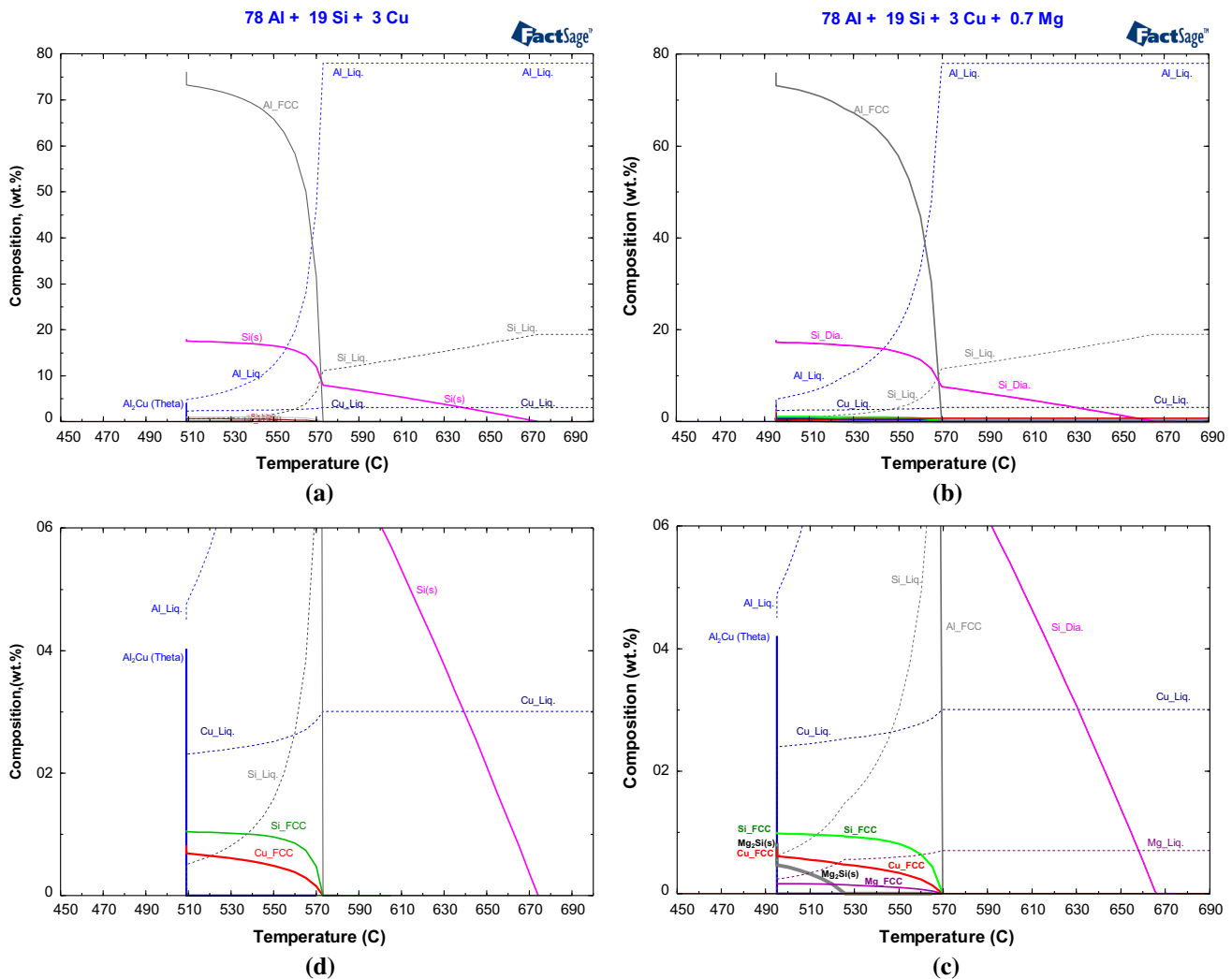


Fig. 6—FactSage calculation of non-equilibrium (Scheil) solidification for Al-19 pct Si-2.8 pct Cu alloy (a, d) and Al-19 pct Si-2.8 pct Cu-0.7 pct Mg alloy (b, c).

time curve (a) and the first derivative of temperature (the instantaneous cooling rate, °C/s) over the temperature range of solidification (b). The changes to the solidification path of the Al-19 pct Si system introduced by the subsequent addition of 2.8 pct Cu followed by 0.7 pct Mg led to notable differences between the cooling curves.

First, it is clear that addition of Cu caused earlier initiation of solid-phase evolution (primary Si), raising the solidus temperature by about 10 K, an effect which can be seen on both Cu-added and Cu-Mg-added alloys, compared to the binary Al-Si alloy (point #1). This can possibly explain visible differences in the refinement of primary Si as a result of Cu and Mg additions (Figure 1).

Second, the additions of Cu and Mg also led to delayed formation of the Al-Si eutectic, *i.e.*, the eutectic temperature shifted from 843 K to 835 K (570 °C to 562 °C) and 830 K (557 °C), for the Cu-added and Cu-Mg-added alloys, respectively (point #2). We note that both of these observations were also confirmed by *in situ* neutron diffraction analysis, which also helped to quantify the amount of primary Si evolution, as is demonstrated later in this paper.

Another effect of the alloying additions can be observed towards the end of solidification, *i.e.*, solidus temperature when minority phases are formed. The energy release within the temperature range of 781 K to 768 K (508 °C to 495 °C) on the Al-19 pct Si-2.8 pct Cu curve (point #3) can only be attributed to Al<sub>2</sub>Cu theta phase formation. Al<sub>2</sub>Cu theta phase formation may also be the cause of the spike in energy release observed around 763 K (490 °C) on the Al-Si-Cu-Mg curve (point #3), because the theta phase is the last solid-phase evolving during solidification of this alloy. This curve, however, has another area of elevated energy release, around 788 K to 783 K (515 °C to 510 °C) (point #3'). According to the phase diagram, and as discussed earlier in this paper, this increase in energy release is likely due to the initiation of Mg<sub>2</sub>Si phase formation.

Finally, the end of solidification, that is, the solidus, can only be clearly observed for the binary Al-Si alloy (point #4) at 815 K (542 °C). For the other two alloys with added Cu or Cu-Mg, the final stage of solidification is smeared by evolution of the minority phases, which are partially solid-state transformations. Regardless of

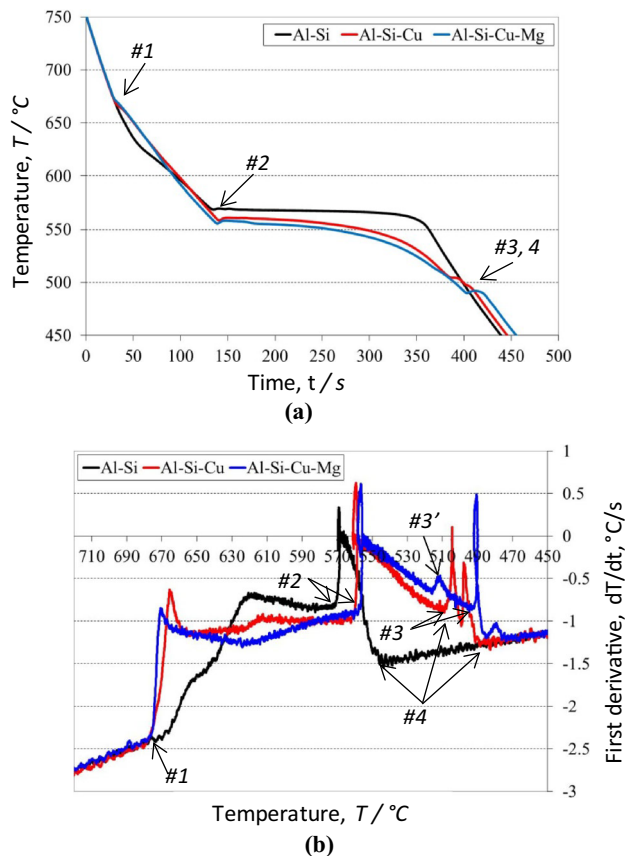


Fig. 7—Thermal analysis results for Al-19 pct Si, Al-19 pct Si-2.8 pct Cu and Al-19 pct Si-2.8 pct Cu-0.7 pct Mg alloys obtained during solidification process from 1023 K to 723 K (750 °C to 450 °C). (a) Temperature vs time cure. (b) Temperature vs 1st derivative curve (cooling rate). Numbered features are referred to in the text.

this “smearing” effect, it is obvious that Cu and Cu-Mg additions significantly reduce solidus temperature, by about 308 K and 318 K (35 °C and 45 °C) for the Cu-added and Cu-Mg-added alloys, respectively.

#### IV. NEUTRON DIFFRACTION ANALYSIS

Neutron diffraction was used for more in-depth analysis of the liquid or mushy zone that is typically unobtainable from classical thermal analysis experiments. A detailed description of the application of neutron diffraction to the analysis of solid-phase evolution is given in our earlier papers.<sup>[23–25]</sup> The main idea of the method is the direct correlation between the normalized intensity of the diffracted monochromatic neutron beam at the specific  $2\Theta$  angular range with the amount of solid phase that has a Bragg’s peak within the same  $2\Theta$  range.

By evaluating the entire 80-deg diffraction spectrum one can retrieve the relative intensity of the Bragg peaks that correspond to the phases that evolve in the solidifying Al-Si alloy. Figure 8 presents diffraction patterns obtained from the binary Al-19 pct Si alloy

when melt temperature was reduced in a stepwise mode from 983 K to 793 K (710 °C to 520 °C).

The neutron diffraction data presented in Figure 8 clearly show the major solid-phase constituents of Al-19 pct Si binary alloy, *i.e.*, primary Si and eutectic Al-Si evolved during solidification process. Closer examination shows that some solid Si already existed in the melt at temperatures of approximately 943 K (670 °C), as long-range atomic scattering was detected around the scattering angles of 28.3, 55.8, and 94.5 deg. For the given neutron wavelength, these scattering angles correspond to Si crystallographic planes of {111}, {311}, and {511}. It is noteworthy that the 943 K (670 °C) liquidus temperature established from the thermal analysis experiments and it is 7 K lower than the one predicted from the thermodynamic calculation.<sup>[24]</sup> The long-range atomic scattering that appears as broad diffraction peaks, indicates the presence of clusters of primary silicon crystallites that may be only several nanometres in length. As temperature is further reduced, the peaks become narrower and taller as the Si clusters grow and form micrometre-sized crystals floating in the melt.<sup>[21–24,31,32]</sup> From the diffraction pattern, it appears likely that the Si crystallites are present in the melt at higher temperatures [most likely exceeding 950 K (677 °C)], but much longer counting time is required to acquire the statistically valid data to support this claim. Verification of this hypothesis may become crucial for proper selection of melt processing and casting parameters, since it affects the size and distribution of Si in the cast component.

Neutron diffraction data also revealed detectable scattering from the following crystallographic planes of Al {111}, {200}, {220}, {311} and {331} recorded for temperature range between 940 K and 928 K (667 °C and 655 °C) (Figure 8). These peaks could indicate that aluminum crystals nucleated prior to the Al-Si eutectic, which contradicts the existing paradigm that  $\alpha$ -Al starts to nucleate simultaneously with Si while forming eutectic phase at approximately 842 K (569 °C) (Figure 7).<sup>[7]</sup> The  $\alpha$ -Al phase was not detected at 898 K and 868 K (625 °C and 595 °C), which indicates that nucleation started at 940 K (667 °C) was discontinued at 898 K (625 °C) and re-started again at the Al-Si eutectic temperature [ $\sim$ 842 K (569 °C)]. Microstructure analysis of the Al-19 pct Si alloy showed randomly distributed  $\alpha$ -Al dendrites (Figure 1(a)). It has to be noted that such widely used techniques as thermal analysis are not capable of directly detecting atoms clustering in the liquid or premature nucleation of  $\alpha$ -Al crystals prior to Al-Si eutectic nucleation. It should also be noted that several Al peaks—{111}, {200}, and {311}—were evolving in close proximity to the “background peaks” coming from materials forming the solidification cell, as it is shown, for example, for the Al {111} peak in Figure 9. Overlapping of the peaks may lead to misreading of the information presented in Figure 8 as premature detection of the  $\alpha$ -Al phase.<sup>[26]</sup>

Figure 10 shows fraction solid development for the Al-19 pct Si alloy obtained from neutron diffraction and



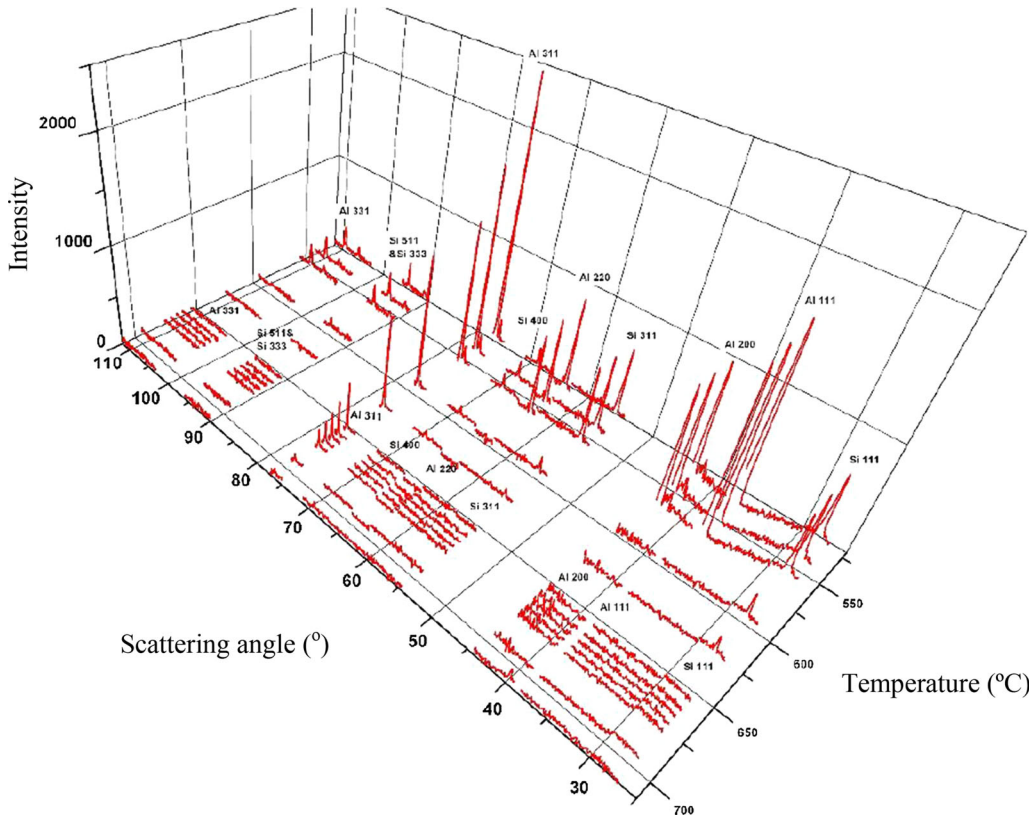


Fig. 8—Neutron diffraction pattern of the Al-19 pct Si binary alloy solidification process collected at various temperatures, ranging from 983 K (710 °C) [311 K (38 °C) above the equilibrium liquidus temperature] to 793 K (520 °C) [293 K (20 °C) below the solidus temperature]. Note that the neutron wave length used in the experiments was 0.155 nm.<sup>[26]</sup>

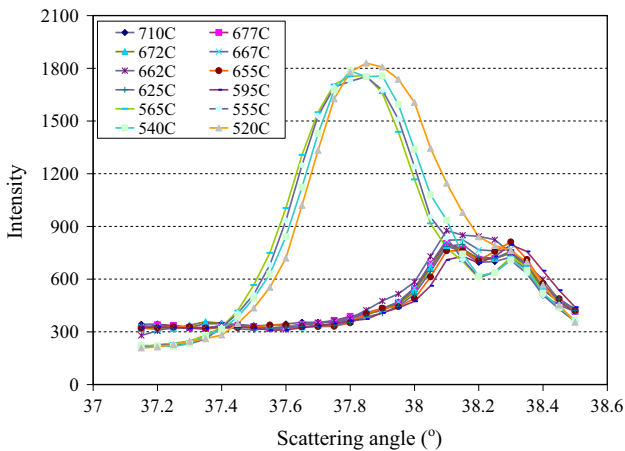


Fig. 9—Evolution of neutron diffraction intensity for Al {111} peak observed in the binary Al-19 pct Si alloy.

thermal analysis during alloy solidification process and indicates a good correlation between these two techniques. The individual fraction-solid profiles for Al and Si, retrieved from the *in situ* experimental data, which are presented in Figure 10, indicate Si atoms clustering in vicinity of liquidus temperature, and the premature nucleation of  $\alpha$ -Al crystals prior to Al-Si eutectic nucleation, *i.e.*, between 940 K and 898 K (667 °C and 625 °C).

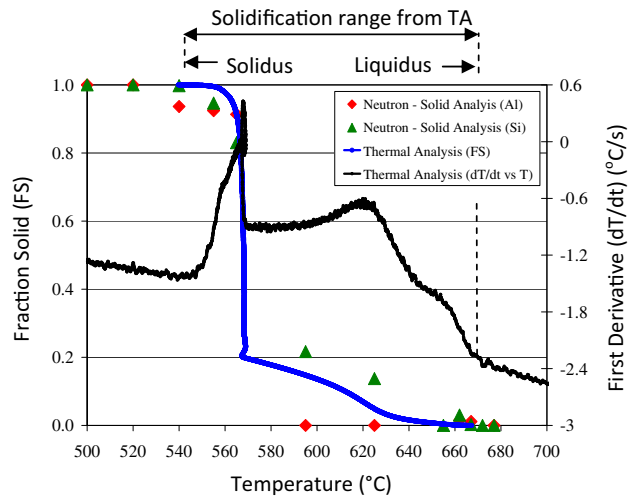


Fig. 10—Integrated data from thermal analysis (fraction solid and derivative curves) and neutron diffraction for the Al-19 pct Si alloy. Neutron diffraction data from solid phase represent averaged integrated diffraction intensity from Si (111, 311, 511, and 333 planes) and from Al (111, 200, 220 and 311) planes.<sup>[24,26]</sup>

Figure 11 depicts the results of comparative analysis for the binary Al-19 pct Si alloy (Figure 11(a)) and Al-19 pct Si-2.8 pct Cu and Al-19 pct Si-2.8 pct Cu-0.7 pct Mg alloys (Figure 11(b)). Similarly to the neutron data presented in Figure 10, based on the intensities of the corresponding Bragg reflections, the figure shows the

evolution of solid  $\alpha$ -Al and solid Si over the temperature range of solidification. Confirming the observations made in the thermal analysis, Figure 11 shows a shift in eutectic temperature, upon addition of 2.8 pct Cu to the original binary Al-Si alloy, towards lower temperature of about 828 K (555 °C) (see Figure 11(b), sample C). Further addition of 0.7 pct Mg shifts the initiation of

the eutectic by 7 to 10 deg farther towards lower temperatures of approximately 818 K to 823 K (545 °C to 550 °C) (Figure 11(b), sample D). The eutectic shift can be observed on both Al and Si curves. As it was already observed in the thermal analysis, the additions of Cu and Mg accelerate evolution of primary Si (Figure 7). The solidification paths presented in Figure 11 confirm and quantify this observation.

The results presented in this paper show the potential of applying neutron diffraction for high-resolution analysis of liquid and semi-solid alloys that can result in new characterization capabilities for detailed studies of grain refining or eutectic modification. This outcome contributes to a better understanding of the solidification behavior of the Al-Si based alloys. Evaluation of the synthetic-type alloys with subsequent addition of Cu and Mg enabled the observation of the individual effects of these alloying elements on the microstructure and mechanical properties. Application of neutron diffraction also allowed detecting phase transformation typically not observed during conventional thermal analysis experiments.

The multi-part analysis performed within scope of this work resulted in various temperatures of nucleation of the Al-Si eutectic, as well as the solidus temperature. These results are summarized in Tables II and III, respectively. Overall, the FactSage computations resulted in about an 8 to 13-deg higher eutectic temperature than that recorded in the thermal analysis and about an 18-deg higher temperature than that observed in the *in situ* neutron diffraction.

There is also no definite answer as to the exact value of the solidus temperature of the alloys (Table III). The FactSage analysis obviously results in different values for the equilibrium and non-equilibrium modes. The detection of solidus temperature in the thermal analysis is complicated by the almost simultaneous evolution of the minority phases ( $\text{Al}_2\text{Cu}$  and  $\text{Mg}_2\text{Si}$ ) at the end of solidification and their corresponding low energy signature. The step-wise approach in the *in situ* neutron diffraction analysis limits the analysis to the pre-specified number of measured temperature points.

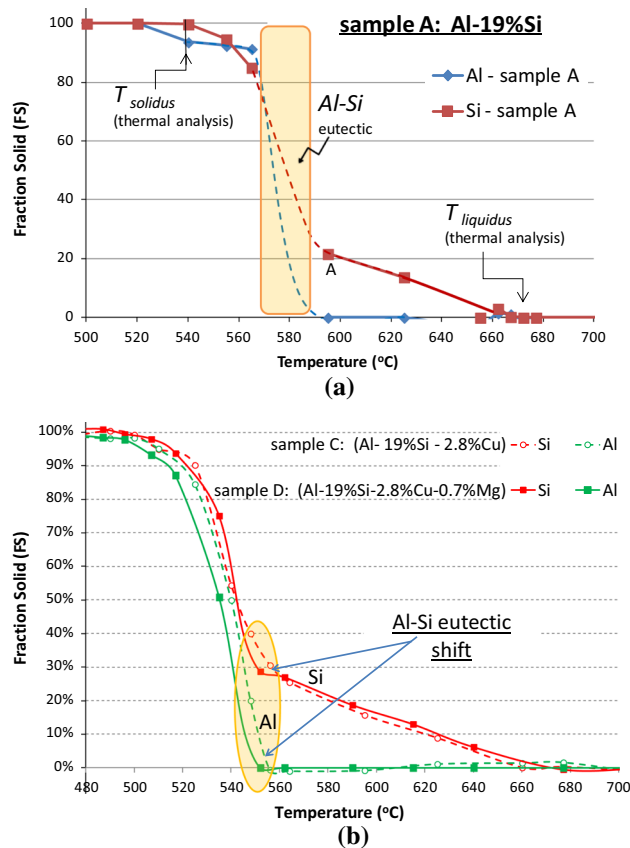


Fig. 11—Solid-phase evolution during solidification of the binary Al-19 pct Si alloy, sample A (a) and Al-19 pct Si-2.8 pct Cu and Al-19 pct Si-2.8 pct Cu-0.7 pct Mg alloys, samples C and D respectively, as determined from the neutron diffraction data (b).

Table II. Temperatures of Nucleation of the Al-Si Eutectic, °C

	Al-19 wt pct Si	Al-Si-2.8 wt pct Cu	Al-19 pct Si-2.8 pct Cu-0.7 pct Mg
FactSage™	577	573	568
Thermal analysis	569	560	555
Neutron diffraction	—	555	550

Table III. Solidus Temperatures, °C

	Al-19 wt pct Si	Al-19 pct Si-2.8 pct Cu	Al-19 pct Si-2.8 pct Cu-0.7 pct Mg
FactSage <sup>(equilibrium)</sup>	578	518	468
FactSage <sup>(Scheil)</sup>	—	508	502
Thermal analysis	542	508/490*	475/495*
Neutron diffraction	—	~500	~480

\*The solidus values obtained in the thermal analysis for the Al-19 pct Si-2.8 pct Cu and Al-19 pct Si-2.8 pct Cu-0.7 pct Mg alloys are considered as estimated values.

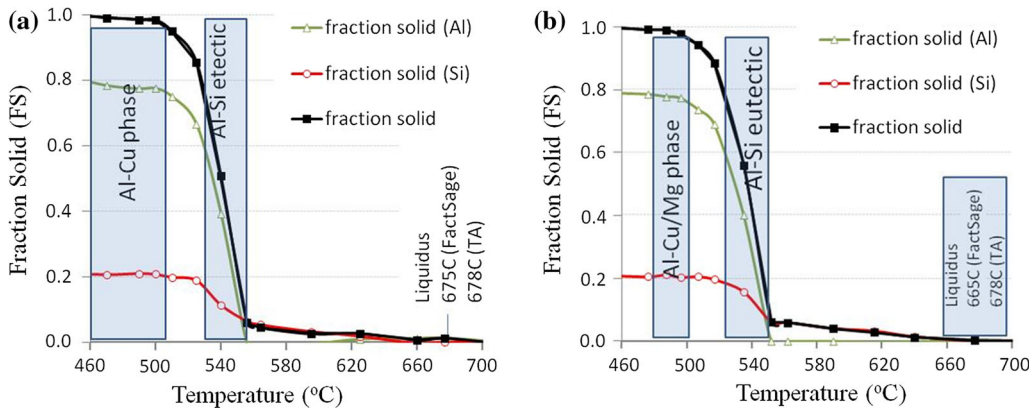


Fig. 12—Fraction solid evolution for the main constituents of the alloys Al-19 pct Si-2.8 pct Cu (a) and Al-19 pct Si-2.8 pct Cu-0.7 pct Mg (b) obtained using neutron diffraction.

Nevertheless, the results of the neutron diffraction analysis for the Cu-Mg-added alloy [753 K (480 °C)] came close to the lower-end solidus range determined in the thermal analysis, and also came close to the solidus value obtained in the equilibrium FactSage calculations. This value is also about 20 deg lower than the solidus temperature observed for the Cu-added alloy [about 773 K (500 °C)].

The good statistics obtained in the neutron diffraction analysis for Al and Si phases allows presenting the data on fraction solid evolution during solidification of Al-Si-Cu and Al-Si-Cu-Mg alloys, Figure 12. Unfortunately, no strong diffraction signal was detected from the minority phases ( $\text{Al}_2\text{Cu}$  theta,  $\text{Mg}_2\text{Si}$ ), although the FactSage calculations suggest there may be up to about 4 pct of  $\text{Al}_2\text{Cu}$  and up to 1.4 pct of  $\text{Mg}_2\text{Si}$  phases that start forming at the end of solidification. These observations may mean that the signal coming from the minority phases was hidden in the background or was not strong enough for statistically viable detection, or both. The temperature ranges for evolution of these phases are shaded in Figure 12. The slight variations in Al and Si content within the shaded areas may be related to the formation of  $\text{Al}_2\text{Cu}$  and  $\text{Mg}_2\text{Si}$ , although a much longer counting time must be used in *in situ* neutron diffraction, to reliably detect the evolution path for these phases.

## V. SUMMARY AND DISCUSSION

Investigation techniques discussed in this study represent broad range of microstructure evolution assessment tools that could be applied by research community. Thermal analysis is known as a well-established laboratory technique, while its application is frequently extended into industrial environments as an on-line metal quality control tool.<sup>[33–35]</sup> The results presented here provide evidence that this technique has potential in reproducing cooling rates in solidification studies, but it may also produce ambiguous results in situations when several phases are evolving simultaneously in the solidifying alloy. This is particularly

evident in the analysis of near-solidus temperature regions of the Al-Si-Cu-Mg alloy system. Evolution of  $\text{Al}_2\text{Cu}$  and  $\text{Mg}_2\text{Si}$  phases, takes place in almost the same temperature range as the solidus temperature (the end of solidification process). Therefore, it is rather difficult to characterize kinetics of the evolution of these intermetallic phases, as well as to establish the solidus temperature accurately. In addition, the cooling rate represents a key factor since it directly affects the temperature gradient across the test sample at non-equilibrium conditions. This could result in a smearing effect in the cooling curve and subsequent difficulties in establishing phase transformation points, particularly for phases that are present in minor quantities. Such behavior might explain differences observed between solidus values recorded by these various techniques [*i.e.*, from 763 K to 791 K (490 °C to 518 °C) as obtained for thermal analysis and neutron diffraction respectively, see Table III].

As a recommendation for future studies, application of *in situ* quenching experiments combined with thermal analysis could bring additional insight as far as microstructure development is concerned. This will include information on the determination of the exact phase transformation temperature as well as quantification of its volume fraction. Phase volume fractions is typically measured using image analysis techniques on test samples quenched from pre-determined temperatures taken along cooling curves plots. This approach, which was not used in this study, was demonstrated by Mackay *et al.*<sup>[36]</sup> for  $\alpha$ -Al dendrite and Al-Si eutectic growth analysis in hypoeutectic Al-Si alloys. As far as quantification of phases is concerned, studies have been performed<sup>[37,38]</sup> where the cooling curve analysis was applied to calculate the total amounts of Cu and Mg based phases that precipitated at the final stages of the solidification process. The total area percentage of the Cu-Mg enriched phases was defined as the ratio of the area between the first derivative of the cooling curve and the hypothetical solidification path of the Al-Si-Cu eutectic to the total area between the first derivative of the cooling curve and the base line. While this approach is novel it still requires further development to account

for various alloy chemistries as well as solidification rate conditions.<sup>[37,38]</sup>

Liquidus temperature determination was not discussed in depth within this work, but it has been demonstrated that application of neutron diffraction brings additional insight on Si atoms clustering in the liquid that most likely took place few degrees above liquidus temperature.<sup>[23–25]</sup> Since quantification of individual phases, *i.e.*, Si and Al during alloy solidification can't be determined accurately by thermal analysis (except by application of quenching experiments), neutron diffraction analysis can help at least partially. As intensity of neutron diffraction is directly related to the evolution of solid phases, the solidus temperature can be identified as the temperature upon which the Al and Si intensities during melt cooling stopped increasing, that is, reached a plateau. This is especially true for the alloying system for which the temperature dependence of the scattering intensities, the Debye–Waller factor, is known.<sup>[39,40]</sup>

Evaluating the kinetics of a secondary phase evolution in neutron diffraction experiments may, however, be greatly complicated by low volume fraction of the phase in the alloy and, therefore, its relatively low scattering intensity. Typically, a neutron diffraction analysis on a phase with a mass fraction below 1 pct is not feasible, as the scattering signal becomes “hidden” in the background. Similar detection limit restriction applies to thermal analysis techniques.<sup>[33,34]</sup> Another complication associated with application of neutron diffraction is a long neutron counting time to acquire a reliable measurement statistics, which leads to a slow, step-wise, cooling of the molten sample during the experiment. This low cooling rate may become too slow to represent contemporary casting technologies used by the industry. But it would be suitable, for example, for studies of sand casting—the processes frequently used in manufacturing of automotive powertrain components such as cylinder blocks and engine heads. Neutron diffraction allows for “observing” these phases individually, as they form during solidification process, therefore not just providing the valuable information of phase evolution, but also eliminating or alleviating the ambiguity in determining the end-of-solidification temperature.

FactSage computations, in general, resulted in higher Al-Si eutectic temperatures than those recorded by the thermal analysis, which are also higher than those observed in the *in situ* neutron diffraction. A detailed explanation of the observed differences among methods used (Table II) is not offered in this work, but potential contributing factors are pointed out. One of them is the differences between solidification conditions, *i.e.*, step-wise cooling for neutron diffraction *vs* continuous cooling for thermal analysis that could affect the initial microstructure condition prior to the Al-Si nucleation. Subsequently, this could relate to differences in the volume fractions of primary Si crystals and  $\alpha$ -Al dendrites as well as saturation of remaining liquid by Si, Cu, Mg atoms, *etc.* Studies reported by Dahle *et al.*,<sup>[41–44]</sup> Zindel *et al.*<sup>[45]</sup> on hypoeutectic alloys, and Talaat *et al.*<sup>[46]</sup> on eutectic alloys pointed out various hypotheses on Al-Si nucleation and growth mechanisms

that could be useful in explaining observed differences in current studies, *i.e.*, (i) Al-Si nucleation on dendrite tips, (ii) eutectic nucleation on the intermetallic phases such as  $\beta$ -(Al,Si,Fe), (iii) eutectic nucleation on AlP nuclei, (iv) as well as for Sr contained alloys and its effect on the Al-Si liquid/solid interface. Some of these factors might be applicable to the investigated alloys since P was used in the studies and the investigated alloys typically contain Fe as impurity element. FactSage calculations do not account for any of the presented mechanisms that might contribute the observed discrepancies on Al-Si eutectic temperature (Table II). In addition, the computational results could differ on chosen mode of solidification (equilibrium *vs* non-equilibrium). In industrial casting processes, however, solidification is rarely equilibrium and its progress is largely dependent on applied cooling rate. No attempt was made to explain this further since extent of this work will be beyond scope of this publication.

In summary, the presented results indicate that four various techniques applied to analyze solidification process of Al-Si alloys (*i.e.*, metallography evaluation, thermal analysis, FactSage computation, and neutron diffraction) have their strength and weaknesses. Their choice of application depends on specific type of analysis, and subsequently instrument access and cost. For in-depth assessments, preferably these methods should be used in the complimentary way in order to eliminate potential errors and misinterpretations.

## VI. CONCLUSIONS

1. The sequential addition of alloying elements (2.8 pct Cu, followed by 0.7 pct Mg) into the high-purity binary Al-19 pct Si alloy with and without P enabled the observation of changes introduced into the solidification pattern by the separate additions.
2. Addition of 0.01 pct P to the Al-19 pct Si binary alloy resulted in refinement of primary Si crystals with subsequent addition of 2.8 pct Cu followed by 0.7 pct Mg.
3. Addition of 0.01 pct P had insignificant effect on hardness (~24 HRB), while 2.7 pct of Cu increased hardness by approximately 25 HRB to a total of 49 HRB, and then 0.7 pct Mg resulted in additional increase of 15 HRB to a total of 64 HRB. A similar trend was observed for as-cast tensile strength where UTS increased from  $91 \pm 2$  MPa for Al-19 pct Si alloy to  $177 \pm 2$  MPa for alloy containing Cu and Mg additions.
4. The various analyses performed resulted in different temperatures of initiation of the Al-Si eutectic. The FactSage computations, in general, result in about 8 to 13 deg higher eutectic temperatures than those recorded in the thermal analysis, and about 18 deg higher temperatures than those observed in the *in situ* neutron diffraction analysis. This finding suggests that the relatively slow cooling during thermal analysis reduced the eutectic temperature of the alloys, and that an even slower, step-wise reduction in temperature during *in situ* neutron diffraction

further delays the initiation of eutectic solidification.

- The various analyses found different values of the solidus temperature of the investigated alloys. Nevertheless, the results of neutron diffraction analysis for the Cu-Mg-added alloy [753 K (480 °C)] came close to the lower-end solidus range determined in the thermal analysis, and also came close to the solidus value obtained in the equilibrium FactSage calculations. This value is also about 20 deg lower than the solidus temperature observed for the ternary Al-Si-Cu alloy [about 773 K (500 °C)].
- The *in situ* neutron diffraction revealed the individual profiles of solid Al and solid Si evolution. The analysis showed that the solid phase was present in the diffraction pattern as solid Si until the temperature reached 813 K (540 °C) for the Al-19 pct Si-2.8 pct Cu alloy and 808 K (535 °C) for the Al-19 pct Si-2.8 pct Cu-0.7 pct Mg alloy, when solid Al was first detected.
- Minority phases may start forming at the end of solidification as predicted by the FactSage calculation (be up to ~4 pct of Al<sub>2</sub>Cu and up to 1.4 pct of Mg<sub>2</sub>Si). However, the neutron diffraction data did not confirm this prediction, possibly because the signal was too weak for a statistically-viable detection of the phases.
- The FactSage computations predicted that the Al<sub>2</sub>Cu theta phase should form following complete solidification of the alloy. This prediction was confirmed by the thermal analysis, as an energy release was detected within the temperature range of 781 K to 765 K (508 °C to 492 °C), which was explained by an enthalpy change associated with the formation of the Al-Cu phase.
- The FactSage computations also predicted that the Mg<sub>2</sub>Si phase should form at the end of solidification of the Al-Si-Cu-Mg alloy. The energy release observed in thermal analysis in the temperature range of around 788 K to 783 K (515 °C to 510 °C) was associated with the initiation of Mg<sub>2</sub>Si phase formation.

## ACKNOWLEDGMENTS

The authors would like to thank Renata Zavadil for assistance with metallographic work and Marta Aniolek MSc. Eng. for thermal analysis experiments. Financial support of the Materials for Energy End Use in Transformation Program of Natural Resources Canada is gratefully acknowledged. Studies completed at the Canadian Neutron Beam Centre (CNBC) were partially sponsored by the Natural Sciences and Engineering Research Council of Canada (NSERC). We gratefully acknowledge contributions made to this study by Drs. Ovidiu Garlea and Clarina de la Cruz, Oak Ridge National Laboratories. Moreover, we thank Ibrahim Sadiq and Matthew Li from University of Waterloo for their help with experimental data processing and graphical data representation during their

co-op terms correspondingly at CanmetMATERIALS and CNBC.

## REFERENCES

- J.L. Jorstad: *AFS Trans.*, 2009, vol. 117, pp. 241–49.
- Y.P. Telang: *AFS Trans.*, 1963, vol. 71, pp. 232–40.
- W. Kasprzak, J.H. Sokolowski, H. Yamagata, M. Sahoo, and H. Kurita: *Int. J. Metalcast.*, 2009, vol. 3 (3), pp. 55–73.
- H. Yamagata, H. Kurita, M. Aniolek, W. Kasprzak, and J.H. Sokolowski: *J. Mater. Process. Technol.*, 2008, vol. 199 (1–3), pp. 84–90.
- H. Yamagata, W. Kasprzak, M. Aniolek, H. Kurita, and J.H. Sokolowski: *J. Mater. Process. Technol.*, 2008, vol. 203, pp. 333–41.
- J.L. Jorstad and D. Apelian: *Int. J. Metalcast.*, 2009, vol. 3 (3), pp. 13–43.
- L.C. Backerüd: *Solidification Characteristics of Aluminum Alloys. Foundry Alloys*, American Foundry Society Inc., Stockholm, 1990, vol. 2.
- N.G. Tenekedjiev: *Cast Met.*, 1990, vol. 3, pp. 96–105.
- J.C. Weiss and C.R. Loper: *Trans. Am. Foundry Soc.*, 1987, vol. 95, pp. 51–62.
- S.M. Ghosh: *AFS Trans.*, 1964, vol. 72, pp. 721–32.
- Y.P. Telang: *Trans. Am. Foundry Soc.*, 1963, vol. 71, pp. 232–40.
- P. Henslar: The New Porsche 944 4-Cylinder Aluminum Engine, SAE Paper, 1983, No. 830004.
- J.L. Jorstad: Reynolds 390 Engine Technology, SAE Paper, 1983, No. 830010.
- H. Kurita, H. Yamagata, H. Arai, T. Nakamura: SAE Technical Paper, SAE World Congress, Detroit, 2004.
- W. Kasprzak, J.H. Sokolowski, H. Yamagata, M. Aniolek, and H. Kurita: *J. Mater. Eng. Perform.*, 2011, vol. 20, pp. 120–32.
- J.L. Jorstad and D. Apelian: *Die Cast. Eng.*, 2004, vol. 48(3), pp. 50, 52, 54–56, 58.
- L.Y. Dehong: *J. Mater. Process. Technol.*, 2007, vol. 189, pp. 13–18.
- H.U. Takagi: *Mater. Trans.*, 2007, vol. 48, pp. 960–66.
- R.-Y. Wang and H.-Y. Lu: *Trans. Am. Foundry Soc.*, 2007, vol. 117, pp. 241–48.
- D. Sediako, F. D'Elia, A. Lombardi, A. Machin, C. Ravindran, C. Hubbard, and R. Mackay: *SAE Int. J. Mater. Manuf.*, 2011, vol. 4, pp. 138–51.
- N. Iqbal, N.H. van Dijk, V.W.J. Verhoeven, W. Montfroof, T. Hansen, L. Katgerman, and G.J. Kearley: *Acta Mater.*, 2003, vol. 51, pp. 4497–4504.
- N. Iqbal, N.H. van Dijk, V.W.J. Verhoeven, T. Hansen, L. Katgerman, and G.J. Kearley: *Sci. Eng. A*, 2004, vol. 367, pp. 82–88.
- W. Kasprzak, D. Sediako, M. Sahoo, M. Walker, and I. Swainson: *Proceedings of TMS 2010, Supplemental Proceedings: Volume 1, Materials Processing and Properties*, pp. 93–104.
- W. Kasprzak, D. Sediako, M. Walker, M. Sahoo, and I. Swainson: *Metall. Mater. Trans. A*, 2011, vol. 42A, pp. 1854–62.
- D. Sediako, W. Kasprzak, I. Swainson, and O. Garlea: *Aluminum Alloys: Fabrication, Characterization and Applications, Supplemental Proceedings: Volume 2: Materials Fabrication, Properties, Characterization, and Modeling*, The Minerals, Metals & Materials Society, TMS, San Diego, CA, February 2011, pp. 279–89.
- W. Kasprzak, D. Sediako, M. Aniolek, and H. Kurita: *13th International Conference on Aluminum Alloys (ICAA13)*, 2013, pp. 1431–40.
- M. Kasprzak, W. Kasprzak, W.T. Kierkus, and J.H. Sokolowski: U.S. Patent No. 7,354,491; Canadian Patent No. 2,470,127, 2009. <http://www.factsage.com>. Accessed Aug 2011.
- E. Sjolander and S. Seifeddine: *J. Mater. Process. Technol.*, 2010, vol. 210, pp. 1249–59.
- L.J. Colley, M.A. Wells, R. MacKay, and W. Kasprzak: *Proceedings of the 26th ASM Heat Treating Society Conference, Cincinnati, OH*, 2011.
- G.I. Eskin and D.G. Eskin: *Z. Metallkde*, 2004, vol. 95 (8), pp. 682–90.
- W. Wang, X. Bian, J. Qin, and S.I. Syliusarenko: *Metall. Mater. Trans. A*, 2000, vol. 31A (9), pp. 2163–68.

33. J. Tamminen: *Thermal Analysis for Investigation of Solidification Mechanisms in Metals and Alloys, Chemical Communications*, University of Stockholm, Stockholm, 1988.
34. L. Bäckerud, G. Chai, and J. Tamminen: *Solidification Characteristics of Aluminum Alloys, Foundry Alloys*, AFS/Skanaluminum, Des Plaines, IL, 1990, vol. 2, pp. 71–84.
35. M. Djurdjevic, H. Jiang, and J. Sokolowski: *Mater. Charact.*, 2001, vol. 46 (1), pp. 31–38.
36. R. Mackay and J. Sokolowski: *Int. J. Metalcast.*, 2008, vol. 2 (2), pp. 77–80.
37. M.B. Djurdjevic, I. Vicario, and G. Huber: *Rev. Metal.*, 2014, vol. 50 (1), pp. 35–46.
38. M.B. Djurdjevic, W. Kasprzak, C. A. Kierkus, W.T. Kierkus, and J.H. Sokolowski: Quantification of Cu Enriched Phases in Synthetic 3XX Aluminum Alloys Using the Thermal Analysis Technique, AFS Transactions, 15th Casting Congress, Dallas, 2001, pp. 1–12.
39. D.B. Sirdeshmukh, L. Sirdeshmukh, and K.G. Subhadra: in *Micro- and Macro-Properties of Solids, Materials Science*, 2006, vol. 80, ISBN: 978-3-540-31785-2, pp 77–133.
40. M.T. Hutchings, P.J. Withers, T.M. Holden, and T. Lorentzen: *Introduction to the Characterization of Residual Stress by Neutron Diffraction*, CRC Press, Boca Raton, 2005.
41. K. Nogita, S.D. McDonald, and A.K. Dahle: *TMS Annual Meeting, SHAPE CASTING: 2nd International Symposium*, Orlando, FL, 2007, Code 73625, pp. 51–58.
42. A.K. Dahle: *5th International Conference on Solidification and Gravity*, Miskolc-Lillafured, Hungary, September 2008, Code 81394, 2010, vol. 649, pp. 287–93.
43. L. Salvo, P. Lhuissier, M. Scheel, S.A. Terzi, M. DiMichiel, E. Boller, J.A. Taylor, A.K. Dahle, and M. Suéry: *Trans. Indian Inst. Met.*, 2012, vol. 65 (6), pp. 623–26.
44. A.K. Dahle, K. Nogita, J.W. Zindel, S.D. McDonald, and L.M. Hogan: *Metall. Mater. Trans. A*, 2001, vol. 32A (4), pp. 949–60.
45. J.W. Zindel, G. Goldewski, and D. Donlon: *Modeling of Casting, Welding & Advanced Solidification Processes VII*, TMS, San Diego, 1998, June 7–12.
46. E. Talaat and H. Fredriksson: *Mater. Trans.*, 2000, vol. 41 (4), pp. 507–15.